BIOCHEMISTRY
including biophysical chemistry & molecular biology
Article

Biochemistry **2009,** *48,* 4031–4039 4031
DOI:10.1021/bi900023m

^{15}N NMR Relaxation Data Reveal Significant Chemical Exchange Broadening in the α-Domain of Human α-Lactalbumin†

Gilles Bruylants‡ and Christina Redfield*

Department of Biochemistry, University of Oxford, South Parks Road, Oxford OX1 3QU, United Kingdom
‡Current address: Molecular and Biomolecular Engineering, Service Matières et Matériaux, CP165/64, Université Libre de Bruxelles, 50 Avenue Franklin D. Roosevelt, 1050 Brussels, Belgium

Received January 7, 2009. Revised Manuscript Received March 19, 2009

ABSTRACT: Human α-lactalbumin (α-LA), a 123-residue calcium-binding protein, has been studied using ^{15}N NMR relaxation methods in order to characterize backbone dynamics of the native state at the level of individual residues. Relaxation data were collected at three magnetic field strengths and analyzed using the model-free formalism of Lipari and Szabo. The order parameters derived from this analysis are generally high, indicating a rigid backbone. A total of 46 residues required an exchange contribution to T_2; 43 of these residues are located in the α-domain of the protein. The largest exchange contributions are observed in the A-, B-, D-, and C-terminal 3_{10}-helices of the α-domain; these residues have been shown previously to form a highly stable core in the α-LA molten globule. The observed exchange broadening, along with previous hydrogen/deuterium amide exchange data, suggests that this part of the α-domain may undergo a local structural transition between the well-ordered native structure and a less-ordered molten-globule-like structure.

Human α-lactalbumin (α-LA)[1] is a 123-residue two-domain calcium-binding protein (Figure 1a); the α-domain, composed of residues 1−39 and 82−123, is largely α-helical, and the β-domain, composed of residues 40−81, contains a triple-stranded antiparallel β-sheet (*1*). This structure is stabilized by four disulfide bridges, two in the α-domain (Cys6-Cys120 and Cys28-Cys111), one in the β-domain (Cys61-Cys77), and one connecting these two domains (Cys73-Cys91). Human α-LA displays significant sequence (∼40%) and structural homology (rmsd of 1.26 Å for 122 C^{α} positions) with hen egg white lysozyme (HEWL) (*1*,*2*). However, despite these similarities human α-LA and HEWL differ in function but also in their stability with respect to pH and temperature (*2*−*5*). The native state of HEWL is stable at pH values ranging from 2 to 10. By contrast, α-LA adopts a native structure homologous to that of HEWL at neutral and alkaline pH but undergoes a partial unfolding transition to a molten globule at acidic pH. Native HEWL unfolds in denaturant or with temperature via a two-step transition whereas α-LA populates a molten globule prior to complete unfolding. The human α-LA molten globule is compact and is characterized by significant native-like helical secondary structure but lacks specific tertiary contacts. This molten globule has a bipartite structure; the α-domain retains native-like helical secondary structure while the β-domain is largely unstructured (*6*−*9*). A close similarity exists between the α-LA molten globule observed at equilibrium at low pH and that formed during the early stages of refolding (*10*−*14*). For this reason, the α-LA molten globule has been used as a model system for characterizing intermediate states in protein folding.

The stable molten globule formed by α-LA at low pH or high temperature has been extensively studied by NMR spectroscopy (*8*,*9*,*15*−*21*) and by other biophysical and computational techniques (*5*,*6*,*22*−*27*). Fewer NMR studies have focused on the native state of the protein (*8*,*13*,*28*−*31*). In particular, the dynamics of the native state have not been studied previously. Here, we have used ^{15}N NMR relaxation methods to characterize, at the level of individual amino acid residues, the backbone dynamics of human α-LA. By collecting ^{15}N longitudinal (T_1) and transverse (T_2) relaxation times and the $\{^1H\}-^{15}N$ heteronuclear NOE values at multiple frequencies, it is possible to obtain a detailed picture of backbone dynamics over a

†Funding from the Wellcome Trust is acknowledged (Grant 079440). G.B. thanks the Fondation Wiener-Anspach and the Belgian FRS-FNRS for postdoctoral fellowships.
*Corresponding author. Tel: +44 1865 275330. Fax: +44 1865 613201. E-mail: christina.redfield@bioch.ox.ac.uk.
[1]Abbreviations: α-LA, α-lactalbumin; rmsd, root-mean-square deviation; HEWL, hen egg white lysozyme; NMR, nuclear magnetic resonance; TOCSY, total correlation spectroscopy; HSQC, heteronuclear single-quantum correlation; NOESY, nuclear Overhauser enhancement spectroscopy; α-LA(β), a two-disulfide variant of human α-LA containing the Cys61-Cys77 and Cys73-Cys91 disulfides but lacking the Cys6-Cys120 and Cys28-Cys111 disulfides.

Published on Web 3/23/2009

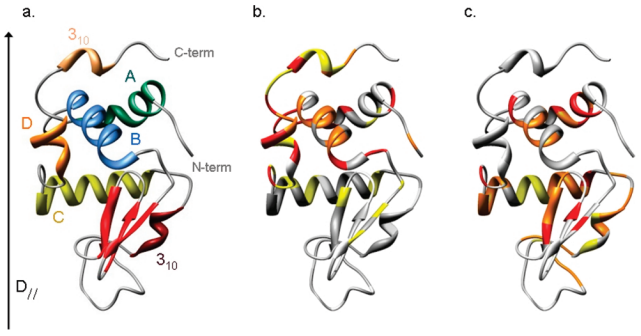

FIGURE 1: (a) 3D structure of human α-LA rendered with UCSF Chimera (*69*) (PDB code 1HML (*47*)). The elements of secondary structure are shown: helices are labeled on the diagram, and the three strands of the β-sheet are represented in red. The direction of the principal component of the diffusion tensor, $D_{||}$, is indicated. (b) Residues requiring model 2 or 4, with an exchange contribution, R_{ex} (S^{-1}), (R_{ex}) to T_2, are shown ($0 < R_{ex} < 1.5$ in yellow, $1.5 \leq R_{ex} < 3.0$ in orange, and $R_{ex} \geq 3.0$ in red). (c) Schematic representation of the hydrogen/deuterium exchange protection factors determined by Schulman et al. (*8*). Residues with protection factors less that 1×10^4 are shown in red, residues with protection factors in the range 1×10^4 to 1×10^5 are shown in orange, and residues with protection factors greater than 1×10^5 are shown in yellow.

large range of time scales, ranging from picoseconds to milliseconds. In contrast to observations for hen and human lysozymes (*32*,*33*), the NMR spectrum of native human α-lactalbumin is characterized by a very large number of exchange-broadened peaks. The majority of these arise from residues in the A-, B-, D-, and C-terminal 3_{10}-helices of the α-domain of the native protein. This observation, along with previous hydrogen/deuterium exchange data, suggests that this part of the α-domain may undergo a local structural transition between the well-ordered native structure and a less-ordered molten-globule-like structure.

MATERIALS AND METHODS

Sample Preparation. Uniformly ^{15}N-labeled recombinant human α-lactalbumin was expressed and purified as described previously (*8*). NMR samples of α-LA were prepared at a concentration of 1 mM at pH 6.3 in 95% H_2O/5% D_2O with 3 mM $CaCl_2$. No significant concentration-dependent changes have been observed in NMR spectra of α-LA obtained at protein concentrations ranging from ~0.3 to ~3 mM. Pulse-gradient spin longitudinal echo diffusion (PG-SLED) experiments have been used previously to determine the hydrodynamic radius (R_s) of the native, molten globule and unfolded states of human α-LA (*34*). The R_s value of 20.6 Å determined for 1 mM human α-LA at pH 6.2 is consistent with the predicted value of ~19.2 Å for monomeric protein (*35*). In addition, solution X-ray scattering experiments have shown that native α-LA is monomeric at concentrations of ~1 mM (*36*).

Assignment of the NMR Spectrum. NMR experiments were performed on a home-built 600 MHz spectrometer equipped with an Oxford Instruments Co. magnet, a home-built triple-resonance probe, and the GE/Omega data acquisition computer and software. The NMR spectrum was assigned using 3D ^{15}N-edited TOCSY-HSQC and NOESY-HSQC data sets (*37*−*39*). The isotropic mixing time in the 3D TOCSY experiment was 24 ms, and a mixing time of 200 ms was used in the 3D NOESY experiment. These were collected with eight scans per increment using 128 complex t_1 (^{1}H) values, 32 complex t_2 (^{15}N) values, and 1024 complex points in the acquisition dimension, t_3 (^{1}H). Sweep widths of 10526.3, 8196.7, and 1730.1 Hz were used in F_3, F_1, and F_2, respectively. A recycle delay of 1.2 s was used in all experiments.

^{15}N NMR Relaxation Experiments. NMR relaxation experiments were performed at 18.2 °C on three home-built spectrometers equipped with triple-resonance probes with ^{1}H operating frequencies of 500.1, 600.2, and 750.2 MHz. The temperature was calibrated using the chemical shift difference between the proton resonances in a neat [^{1}H]methanol sample. Pulse sequences for the measurement of the longitudinal (T_1) and transverse (T_2) relaxation times and the $\{^1H\}-^{15}N$ heteronuclear NOE of the backbone ^{15}N nuclei have been described previously (*40*−*42*). T_1 measurements were performed using a series of nine experiments with relaxation delays ranging from 20 to 1106 ms at 500 MHz, from 20 to 1206 ms at 600 MHz, and from 20 to 1506 ms at 750 MHz. T_2 measurements were performed using a series of eight experiments with relaxation delays ranging from 8.8 to 211.0 ms at 500 and 600 MHz and from 20.0 to 157.8 ms at 750 MHz. The CPMG delay ($2\tau_{cp}$) for these experiments was set to 1 ms. The $\{^1H\}-^{15}N$ NOE experiments were recorded at 500 and 750 MHz; spectra were collected with and without ^{1}H saturation for 3.5 s at 500 MHz and 5 s at 750 MHz. Recycle delays were as follows: 2 s at 500 MHz, 4 s for T_1 and 2 s for T_2 at 600 MHz, and 4 s for T_1 and 3 s for T_2 at 750 MHz. The data sets were acquired using 110, 128, and 150 complex t_1 increments with ^{15}N sweep widths of 1091.7, 1308.9, and 1634.0 Hz at ^{15}N frequencies of 50.69, 60.83, and 76.02 MHz, respectively. Complex data points (2K) were recorded in the F_2 dimension at 500 and 600 MHz with sweep widths of 10000.0 and 12048.2 Hz, respectively. Complex data points (4K) were recorded in F_2 at 750 MHz with a sweep width of 25000.0 Hz. At least 16 scans were collected per t_1 increment for T_1 and 32 scans per t_1 increment for T_2. A total of 128 and 96 scans were collected for the $\{^1H\}-^{15}N$ NOE experiments at 500 and 750 MHz, respectively.

Determination of T_1, T_2 and $\{^1H\}-^{15}N$ NOE Ratios. ^{15}N T_1 and T_2 values and $\{^1H\}-^{15}N$ NOE ratios were measured for 106 of the 123 residues of α-LA. HSQC peaks for Cys6, Gly51, Leu105, and Lys108 have not been assigned, Gly19, Leu52, Ser64, and Glu121 give rise to very weak peaks, and Asn44, Asn71, Asp78, Lys79, Asp82, and Ala92 give rise to overlapping peaks. T_1 and T_2 were fitted as single-exponential decays to the peak intensities determined as a function of the eight or nine delay times. The $\{^1H\}-^{15}N$ NOE was calculated as the ratio of the peak intensities in the spectra recorded with and without ^{1}H saturation. Peak heights were determined using in-house peak-picking software. Uncertainties in the T_1, T_2, and $\{^1H\}-^{15}N$ NOE values were estimated from 500 Monte Carlo simulations using the baseline noise as a measure of the error in the peak heights. Repeats of the first time point in T_1 and T_2 experiments confirmed that baseline noise gave a good estimate of

experimental error. The goodness of fit of the T_1 and T_2 data to the single-exponential decay function was assessed by comparing the calculated χ^2 value to χ^2 values at 95% confidence levels. For the T_1 data collected at 500, 600, and 750 MHz, χ^2 values for 98, 102, and 102 residues, respectively, indicated that the T_1 data were adequately fit by the two-parameter decay curve. For the T_2 data collected at 500, 600, and 750 MHz, 86, 91, and 103 residues, respectively, were adequately fit by the two-parameter model. For all six data sets, the sum of the χ^2 values for the 106 residues was less than the sum of the χ^2 values at 95% confidence levels. The fitted ^{15}N T_1, T_2, and $\{^1$H$\}-^{15}$N NOE values and experimental errors are included in Supporting Information Table 1.

Determination of the Axially Symmetric Diffusion Tensor. α-LA has a near-cylindrical shape (Figure 1), and the relaxation data should, therefore, be analyzed with an axially symmetric rotational diffusion tensor (*43*). This tensor was determined by comparison of experimental T_1/T_2 ratios with those calculated using the Lipari−Szabo formalism (*44*,*45*) with spectral density functions appropriate for axially symmetric rotational diffusion (*46*). The magnitudes ($D_\parallel$, $D_\perp$) and orientation (θ, ϕ) of the principal components of the rotational diffusion tensor were searched to optimize the agreement between experimental and calculated T_1/T_2 ratios using the 1.7 Å 1HML X-ray structure (*47*). Calculations of the T_1/T_2 ratio were carried out with a fixed S^2 value of 0.9, an N−H bond length of 1.02 Å, and a ^{15}N chemical shift anisotropy, ($\sigma_\parallel - \sigma_\perp$), of −170 ppm. The principal component of the ^{15}N chemical shift tensor was assumed to lie in the peptide plane and to form an angle of 19° with the N−H bond vector (*48*−*50*). Residues for which the T_1/T_2 ratios are affected by fast or slow molecular motions should be discarded from this analysis; these were identified in an iterative manner. Initially, residues with an NOE ratio below 0.7 at both 500 and 750 MHz, indicative of significant fast time-scale internal dynamics, or with a T_1/T_2 ratio more than one standard deviation above the mean, indicative of millisecond to microsecond chemical exchange broadening, were excluded. The diffusion tensor determined in this way was used for analysis of the relaxation data as described below. Only residues for which the T_1, T_2, and NOE data could be analyzed satisfactorily without a significant R_{ex} or τ_e term were selected for the final round of diffusion tensor optimization. For α-LA this leads to the rejection of the majority of residues in the α-domain (rejection of 47 of the 72 residues for which experimental data are available in this domain) due to significant fast mobility or chemical exchange broadening; the diffusion tensor used in the model-free analysis described below was determined using T_1/T_2 ratios for 48 residues. Analysis of the T_1/T_2 ratios at 500, 600, and 750 MHz resulted in slightly different overall rotational correlation times, $\tau_R = (2D_\parallel + 4D_\perp)^{-1}$, of 10.6, 10.4, and 10.1 ns, respectively. These differences may have arisen due to differing contributions of radiation damping at the three fields to a distortion of the temperature calibration based on a neat [^{1}H] methanol sample (*51*). In order to correct for this, a scaling factor for each field was used in the simultaneous fitting of the diffusion tensor to the T_1/T_2 data collected at the three fields; a final value of 1.295 was obtained for the $D_\parallel/D_\perp$ ratio.

Model-Free Analysis of Relaxation Data. Relaxation data were analyzed using an in-house computer program; this incorporates the model-free formalism of Lipari and Szabo (*44*,*45*), using spectral density functions appropriate for axially symmetric rotational diffusion (*46*) and noncollinearity of the N−H bond vector and the principal component of the ^{15}N chemical shift tensor (*49*), with model selection and Monte Carlo error estimation as described by Mandel et al. (*52*). The relaxation data were fitted using five models: S^2 only (model 1), S^2 and R_{ex} (model 2), S^2 and τ_e (model 3), S^2, R_{ex}, and τ_e (model 4), and the extended model of Clore et al. (*53*) with S_f^2, S_s^2, and τ_s (model 5). S^2 is the generalized order parameter, R_{ex} is the chemical exchange contribution to T_2, and τ_e is the effective correlation time for internal motion on a fast time scale. S_f^2, S_s^2, and τ_s, used in model 5, are the order parameters for faster and slower time-scale motions and the effective correlation time for slow internal motion, respectively; τ_f, the internal correlation time for fast motion in the extended model, was assumed to be sufficiently small and, therefore, not to contribute significantly to the relaxation parameters (*53*). In models 2 and 4, a single R_{ex} term was used to fit the three T_2 values for each residue, and this R_{ex} term was scaled with the field strength by a factor $(B_0/B_{ref})^\alpha$, with B_{ref} = 500 MHz. Initially, values of α = 0, 1, and 2 were tested; for the majority of residues the best fits were obtained with α = 2, indicating a quadratic dependence of exchange broadening on the field strength (*54*). Factors were introduced in the spectral density functions to scale the values of $D_\parallel$ and $D_\perp$ to take into account the small deviations between data sets recorded at different field strengths due to temperature variation (see above). For each model, best fits for S^2 and other relevant parameters (R_{ex}, τ_e, S_f^2, S_s^2, and τ_s) were determined by minimizing the χ^2 parameter using a downhill simplex algorithm (*55*). The error in these parameters was estimated from 1000 Monte Carlo simulations (as one standard deviation from the mean value). The statistical significance of an improvement in χ^2 when a model with m parameters is used instead of a simpler model with n parameters ($m > n$) was assessed with an F-statistic:

$$F = \frac{(\chi_m^2 - \chi_n^2)(N-m)}{\chi_n^2(n-m)}$$

where χ_m^2 and χ_n^2 are for the models with m and n degrees of freedom, respectively, and N is the number of observations, in this case 8. A more complex model was considered to be statistically significant if a p-value of less than 0.2 was obtained from the F-statistic (*52*). The fitted S^2, R_{ex}, and τ_e values are included in Supporting Information Table 2.

RESULTS

Resonance Assignment. The $^1H^N$ and ^{15}N NMR resonances of 116 of the 123 residues of human α-lactalbumin were assigned using the standard sequential assignment approach (Supporting Information Figure 1). Three-dimensional ^{15}N-edited TOCSY-HSQC and

NOESY-HSQC spectra provided the necessary through-bond and through-space correlations. The assignment of the α-LA spectrum was significantly more difficult than that of the spectra of the homologous proteins hen and human lysozyme (*56*,*57*) because there are a large number of broad resonances in the spectrum of α-LA, particularly for residues arising from the B- and D-helices of the α-domain (Supporting Information Figure 1). Cross-peaks arising from Leu105 and Lys108, located in the D-helix, have not been identified here and are presumably broadened beyond detection. Resonances from these residues are also missing in the NMR spectra of bovine and guinea pig α-lactalbumin (*13*,*30*). The assignments have been deposited in the BioMagRes data bank (BMRB entry ID 15892), and the $^{1}H^{N}$ and ^{15}N chemical shifts are included in Supporting Information Table 3.

Analysis of ^{15}N Relaxation Data. ^{15}N T_1 and T_2 values were measured at 500, 600, and 750 MHz and $\{^{1}H\}-^{15}N$ heteronuclear NOE values at 500 and 750 MHz for 106 of the 123 residues of α-LA; these data are included in Supporting Information Table 1. The T_1/T_2 ratios at 500 and 750 MHz are shown in Figure 2a. As expected, ^{15}N T_1 values increase with frequency while T_2 values show more complex frequency dependencies. It is clear from the T_1/T_2 ratios, particularly at 750 MHz, that extensive exchange contributions to T_2 are observed for residues in the α-domain of the protein, particularly for residues 10−40 and 100−120. $\{^{1}H\}-^{15}N$ NOE ratios determined at 500 and 750 MHz are shown in Figure 2b. For the majority of residues, NOE ratios above 0.75 are observed, indicating a rigid backbone, characteristic of a globular protein with limited amplitude dynamics on a fast time scale; similar observations have been made previously for the homologous proteins hen and human lysozyme (*32*,*33*).

α-LA has a near-cylindrical shape (Figure 1) which will give rise to anisotropic rotational diffusion that will affect observed T_1 and T_2 values. Neglecting this anisotropy and assuming isotropic rotation can introduce errors in the interpretation of T_1/T_2 ratios particularly at high magnetic fields (*43*). These ratios can be wrongly interpreted in terms of millisecond to microsecond time-scale motions for residues with elevated T_1/T_2 ratios and in terms of fast picosecond motions for residues with lower T_1/T_2 ratios (*43*). The orientation and magnitude of the principal components of the rotational diffusion tensor were determined as described in Materials and Methods. A group of 48 residues, 35 of which are located in the β-domain or C-helix, were used for the analysis of rotational diffusion anisotropy. Simultaneous fitting of the T_1/T_2 ratios at three frequencies gave a $D_{\parallel}/D_{\perp}$ ratio of 1.295.

T_1/T_2 ratios at 600 MHz calculated using the optimized diffusion tensor are compared with experimental values in Figure 3. The use of an axially symmetric diffusion model gives a clear improvement compared to an isotropic model. A fully anisotropic model was also tested, but this was not found to give a statistically significant improvement to the χ^2 between experimental and calculated T_1/T_2 ratios. It can be seen clearly in Figure 3 that the elevated T_1/T_2 ratios observed for residues 77−85 are due to the parallel orientation of the N−H vectors of these residues, which are located in or adjacent to a 3_{10}-helix (Figure 1a), with respect to the long axis of the protein rather than to a chemical exchange contribution to T_2. The residues preceding and following this region have significantly lower T_1/T_2 values as a result of the perpendicular orientation of the N−H vectors of these residues with respect to the long axis of α-LA (Figure 1a). Residues such as 45 and 46, which were excluded from the T_1/T_2 analysis on the basis of reduced NOE values, show experimental T_1/T_2 ratios that are substantially lower than those predicted on the basis of rotational diffusion anisotropy alone. By contrast, residues such as Tyr36 and

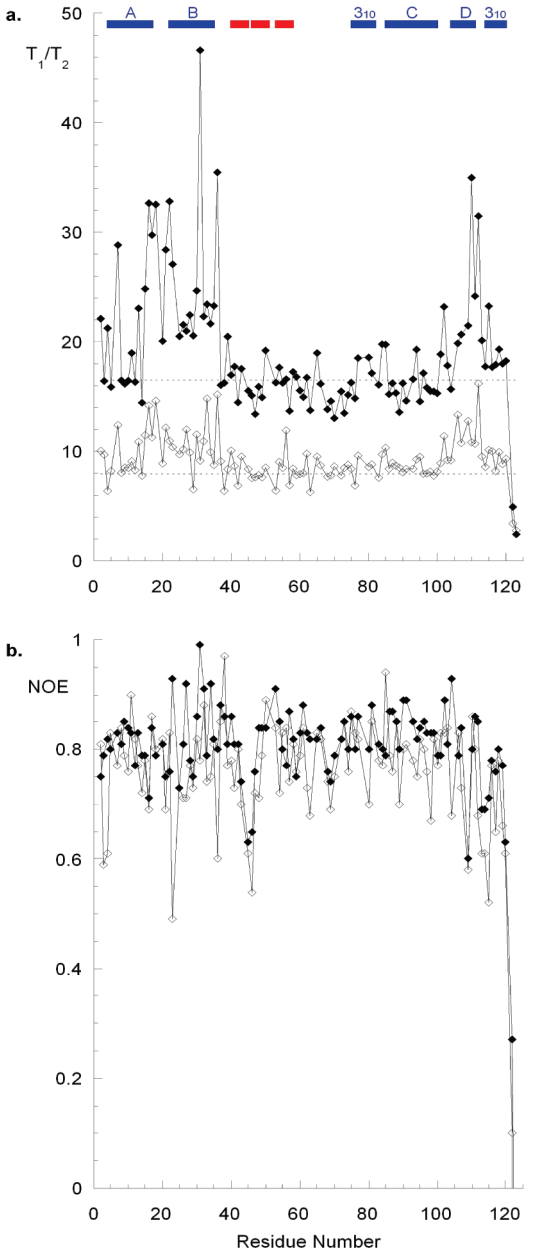

FIGURE 2: (a) Experimental T_1/T_2 ratios obtained at 750 MHz (◆) and at 500 MHz (◇). Dashed lines at 16.50 and 7.94 indicate the predicted T_1/T_2 ratio using an isotropic diffusion model at 750 and 500 MHz, respectively. α-Helices and β-strands are represented by blue and red bars, respectively. (b) Experimental $\{^{1}H\}-^{15}N$ NOE ratios obtained at 750 MHz (◆) and 500 MHz (◇). NOE ratios of −0.17 and −0.72 obtained at 750 and 500 MHz, respectively, for Leu123 are not shown. Experimental errors for the T_1, T_2, and $\{^{1}H\}-^{15}N$ NOE are reported in Supporting Information Table 1.

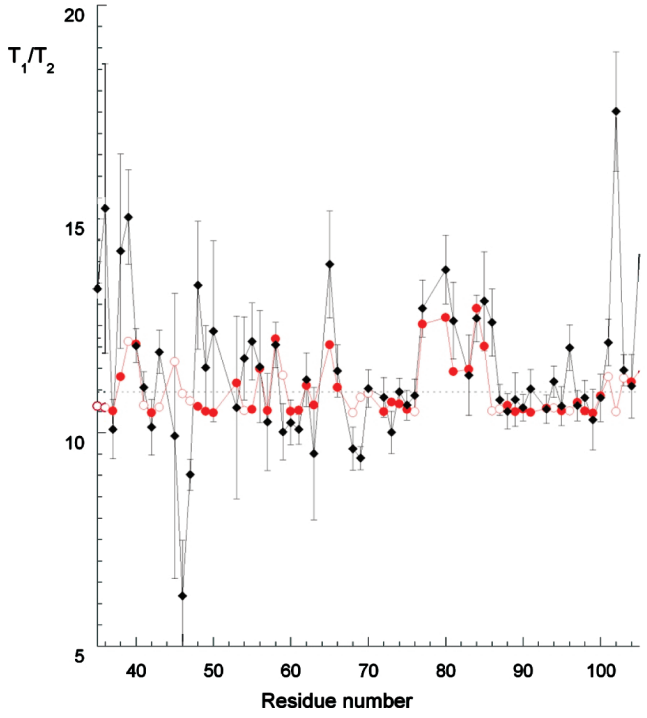

FIGURE 3: Experimental (black rhombus) and predicted (red circles) T_1/T_2 values at 600 MHz for residues 35−105 calculated using the values of $D_{\|}$, $D_{\perp}$, θ, and ϕ obtained using a selected set of 48 residues (filled red circles) for which the T_1/T_2 ratio is not affected by molecular motion. Errors for the experimental T_1/T_2 values are shown. The dashed line at 10.95 represents the constant T_1/T_2 ratio obtained using an isotropic diffusion model.

Asp102, which show substantially higher T_1/T_2 ratios than predicted from rotational diffusion anisotropy, also show field-dependent T_2 values that are characteristic of exchange broadening (Figure 2a).

The axially symmetric diffusion tensor derived from the experimental T_1/T_2 ratios was used for the model-free analysis of the relaxation data (*44*,*45*). Five different models were tested as described in Materials and Methods, and the results are summarized in Supporting Information Table 2. For 88 of the 106 residues for which relaxation data were measured, the model with the fewest parameters that gave a statistically significant χ^2 value which was below the 0.95 critical χ^2 value was selected (*52*). For the 18 remaining residues, none of the five models obeyed this criterion, and the simplest model giving a good fit was selected. Overall, the sum of the χ^2 values for all 106 residues was below the sum of the critical χ^2 values. Model 1 (S^2 only) was selected for 45 of the residues, 34 residues required S^2 and R_{ex} (model 2), 13 required S^2 and τ_e (model 3), 12 required S^2, R_{ex}, and τ_e (model 4), and 2 residues, Lys122 and Leu123 at the C-terminus, required the use of the extended model with S_s^2, S_f^2, and τ_s (model 5). Eight experimental measurements were used in the fitting procedure (T_1 and T_2 at 500, 600, and 750 MHz, $\{^1H\}-^{15}N$ NOE at 500 and 750 MHz) so a statistical *F*-test could be used for model selection for all residues; the number of degrees of freedom ranged from seven for model 1 to five for models 4 and 5 (*52*).

The order parameters (S^2) obtained from the model-free analysis are plotted as a function of sequence in Figure 4. Generally, high S^2 values (>0.8) are obtained for the majority of residues in native α-LA, indicating a rigid backbone. Some residues, for which model 1 gives a satisfactory fit, have very high S^2 values (for example, $S^2 > 0.98$ for Ser9, Tyr18, Ile72, Ile75, and Asp88). These S^2 values could have been decreased by the use of model 2 (S^2 and R_{ex}); however, because of relatively large experimental errors, the use of this latter model was not found to be statistically significant using the *F*-test. The two C-terminal residues have low order parameters of 0.35 and 0.26; these correlate with the high temperature factors (>65 Å^2) in the 1HML X-ray structure of the protein (*47*). Lower order parameters are also observed for residues Asn45 and Glu46 in the β-domain. These residues are located in a turn between two β-strands on the surface of the protein and are also observed to have higher than average temperature factors in X-ray structures (*1*,*47*,*58*).

The chemical exchange contributions (R_{ex} values) are plotted as a function of sequence in Figure 4. It is interesting to note that 43 of the 46 residues in α-LA which require an exchange contribution to T_2 are located in the α-domain of the protein. The largest R_{ex} values (≥ 3.0) are obtained for residues in the A- and B-helices, in the AB loop connecting these helices, and in the D- and C-terminal 3_{10}-helices (Figure 1). Large R_{ex} terms are not observed in the C-helix of the α-domain or in the β-domain. R_{ex} contributions are observed for the majority of residues in the B-helix but not for Thr29 or Phe31. The observation of very weak cross-peaks for these residues in the HSQC spectrum (Supporting Information Figure 1) is likely to arise from shorter $^1H^N$ T_2 values resulting from chemical exchange.

We tested the magnetic field dependence of the chemical exchange contribution, R_{ex}. This term was scaled by a factor $(B_0/B_{ref})^{\alpha}$, with $B_{ref} = 500$ MHz, and three cases were considered: (i) $\alpha = 0$, (ii) $\alpha = 1$, and (iii) $\alpha = 2$. The quadratic dependence ($\alpha = 2$) gave the lowest χ^2 value for most residues, implying that the fast exchange limit is valid, i.e., that $k_{ex}/\Delta\omega \gg 1$ (where k_{ex} is the exchange rate constant and $\Delta\omega$ the difference in angular frequency between the chemical shifts in the two states) (*54*,*59*). For Ile27, Met30, and Thr33, located on one side of the B-helix, and for Ala106 and Cys111, in the D-helix, a linear dependence on field strength ($\alpha = 1$) was found to give the best fit; however, fits with $\alpha = 2$ did give χ^2 values below the 0.95 critical χ^2 value. For these residues exchange may be intermediate on the chemical shift time scale (*54*). This does not necessary mean that the exchange rate (k_{ex}) is different for these residues because the difference in chemical shift between the signals in the two interconverting species must also be considered. It may be that Ile27, Met30, Thr33, Ala106, and Cys111 are characterized by larger chemical shift differences than other residues involved in the exchange process.

Previously, Phan et al. (*59*) have used plots of $(1/T_2 - 1/2T_1)$ versus B_0^2 to identify residues with chemical exchange contributions in the fast exchange limit; residues with R_{ex} contributions show linear plots with steeper gradients than observed for nonexchanging residues. A similar analysis has been carried out for human α-LA (Figure 5). Asp16, Gly20, Ile21, and Leu115 show linear plots with gradients that differ from the average behavior for the

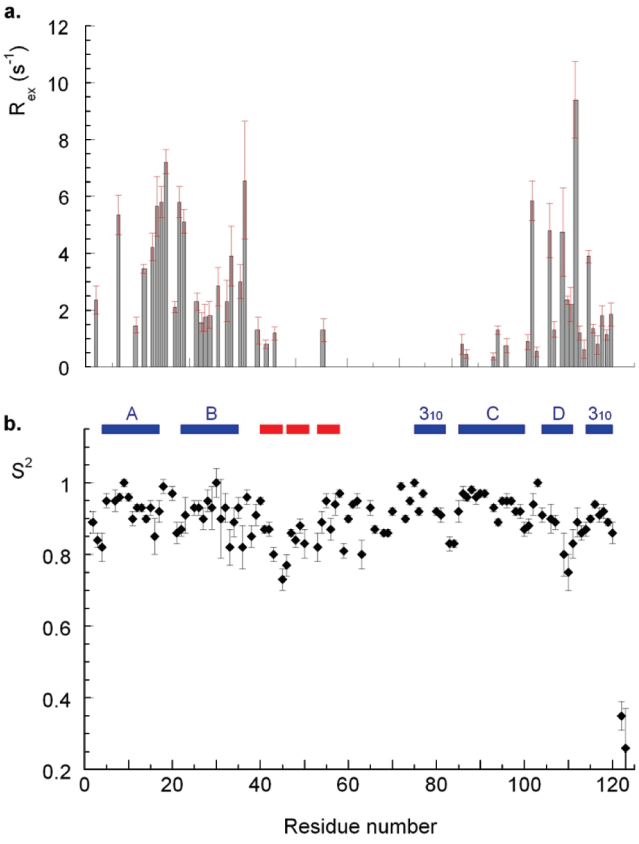

FIGURE 4: (a) R_{ex} and (b) S^2 parameters obtained from the fitting of the ^{15}N relaxation data using the model-free approach, as described in the Materials and Methods section. Errors derived from the Monte Carlo analysis are shown. α-Helices and β-strands are represented in (b) by blue and red bars, respectively.

residues that are not affected by chemical exchange. The linear dependence of these plots confirms the fast chemical exchange limit for these residues (*59*).

DISCUSSION

Using ^{15}N NMR relaxation methods, we have characterized the backbone dynamics of the native state of human α-lactalbumin at the level of individual residues. Relaxation data were collected at three magnetic field strengths for 106 residues and analyzed using the model-free formalism of Lipari and Szabo (*44*,*45*) with spectral density functions appropriate for axially symmetric rotational diffusion (*46*,*49*). Order parameters, S^2, greater than 0.8 are obtained for 100 of 106 residues in native α-LA. Similar behavior has been observed previously for the homologous proteins hen and human lysozyme (*32*,*33*). Lower order parameters are observed for Asn45 and Glu46 in the β-domain and for the two C-terminal residues, Lys122 and Leu123; this is consistent with the higher *B*-factors observed for these residues in X-ray structures (*47*,*58*). Lower order parameters are observed for the homologous residues in HEWL; for example, Thr47 of HEWL, which corresponds to Asn45 in α-LA, has an S^2 value of 0.78 (*32*). The C-helix has the highest average S^2 value (0.95 compared to 0.89 for the entire protein); in HEWL, this helix also has the highest average S^2 value (0.91 compared to 0.87 for the entire protein) (*32*). Overall, the order parameters determined for α-LA suggest a rigid polypeptide backbone throughout the structure with only small amplitude fluctuations on a fast time scale.

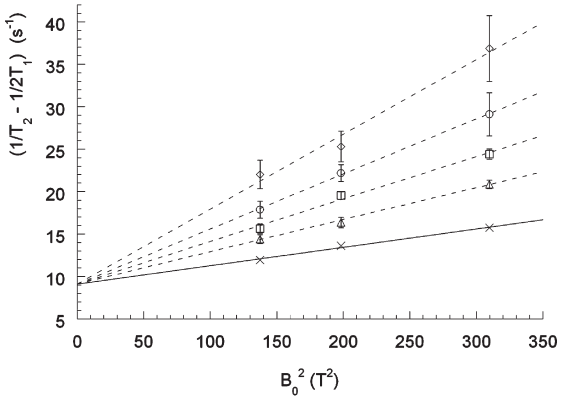

FIGURE 5: Representative plots of $(1/T_2 - 1/2T_1)$ versus B_0^2 for four selected residues illustrate the quadratic dependence of R_{ex} on B_0. Experimental values are shown for Asp16 (◇), Gly20 (△), Ile21 (○), and Leu115 (□). Average values obtained for the 45 residues for which T_1 and T_2 are not affected by molecular motions are shown as crosses. For clarity, and as done by Phan et al. (*59*), all the fitted data sets have been scaled to the same *y*-intercept (that of the fit for the average of the nonexchanging residues) so that only differences in the slope are shown.

A total of 46 residues in α-LA required an exchange contribution (R_{ex}) to T_2. This is in marked contrast to HEWL for which only 3 residues require an R_{ex} term when axially symmetric rotational diffusion is considered (G. Bruylants and C. Redfield, unpublished results) (*60*). Therefore, although the fast time-scale dynamics of α-LA and HEWL appear to be quite similar, the slower millisecond to microsecond time-scale dynamics show a very significant difference. In α-LA, 43 of the 46 residues with exchange broadening are located in the α-domain of the protein. The 28 residues with R_{ex} values of greater than 1.5 are all located in the α-domain and specifically in the A-, B-, D-, and C-terminal 3$_{10}$-helices and in the AB loop (connecting the A and B helices) (Figure 1). This clustering of residues requiring an exchange term suggests a common mechanism for exchange broadening in α-LA.

Hydrogen/deuterium exchange protection factors have been reported for the backbone amide protons of native human α-LA at pH 6.3 and 15 °C (*8*). Protected amides are observed for hydrogen-bonded residues located in both the α-domain and the β-domain. The highest protection factors are observed for residues in the C-helix of the α-domain and close to disulfide bonds in the β-domain; protection factors of greater than 10^5 are observed for 4 residues in the C-helix (Cys91, Ala92, Lys93, and Lys94) and for Cys61, Cys73, Cys77, and Phe80 in the β-domain. Lower levels of protection are observed for other α-domain residues; the average protection factor for residues in the A-helix is 1×10^4 (6 residues) and for the B-helix is 5×10^4 (5 residues). No protection is detected for the D- and C-terminal 3$_{10}$-helices of human α-LA (*8*). A similar pattern of protection is observed for the native state of bovine α-LA (*13*); protection factors of 10^5 and higher are observed for many residues in the β-domain, and values greater than 10^7 are observed in the C-helix. No protection factors greater than 10^5 are observed for the A-, B-, D-, and C-terminal 3$_{10}$-helices of native bovine α-LA (*13*). The lower protection factors observed in the

A-, B-, D-, and C-terminal 3_{10}-helices of α-LA correlate with the observation of R_{ex} contributions for these regions of the structure (Figure 1b,c).

The pattern of hydrogen/deuterium exchange observed in hen and human lysozymes differs from that observed for human and bovine α-LA. Both hen and human lysozymes show more uniform protection factors throughout the structure. For lysozyme, protection factors of greater than 10^6 have been reported for residues in the A-, B-, and C-helices of the α-domain and in the β-domain; protection factors for amides in the C-helix and β-domain are not significantly higher than those observed in the A- and B-helices (*61*,*62*). No significant chemical exchange broadening is observed in either domain of HEWL.

Human α-LA is known to crystallize in two forms; rod-like crystals are obtained at room temperature at pH 4.2 (LT form) and plate-like crystals are obtained at 37 °C at pH 6.5 (HT form) (*63*). These two forms show no significant difference in structure for residues 1−95, but differences are observed for residues 96−123. The largest differences are observed for residues Trp104 to Cys111. These residues adopt an α-helical structure with His107 buried in the pH 6.5 HT form whereas this region forms a loop with His107 exposed to solvent in the pH 4.2 LT form. At pH 6.5 at room temperature, conditions similar to those used in our NMR study, both crystal forms are found, suggesting that under these conditions the two conformations interconvert in solution (*63*). This structural transition, occurring on a millisecond to microsecond time scale, may explain the exchange broadening observed for Ala106, His107, Ala109, Leu110, and Cys111 and the absence of HSQC peaks for Leu105 and Lys108. It may also explain the lack of observed protection for D-helix amides; although the amides of Ala109, Leu110, and Cys111 are hydrogen bonded in the HT form, no hydrogen bonds exist in the LT form. Cys28 in the B-helix is disulfide bonded to Cys111, and several residues in the B-helix make contacts with Trp104−Cys111. The carboxyl group of Glu25 has a polar contact with the side chain of His107 in the HT form but not in the LT form (*63*). Thus, exchange broadening of B-helix residues may arise from differences in chemical shifts arising from changes in these long-range contacts in the two conformations.

The structural transition for residues 104−111 does not, however, explain the more widespread exchange broadening observed for the A-helix and the C-terminal 3_{10}-helix or the reduced protection factors observed for amides in the A- and B-helices. Residues in the A- and C-terminal 3_{10}-helices do not make contacts with residues Trp104−Cys111 (Figure 1). In addition, no changes in hydrogen bonding or solvent accessibility are observed for the A- and B-helices in the two structures (*63*). It may be that in solution α-LA undergoes a more substantial structural perturbation or samples a larger ensemble of conformations in order to accommodate the transition between the two local structures for residues 104−111 that are trapped in the two crystal forms. This may involve significant changes in the environments of the A-, B-, and C-terminal 3_{10}-helices, in addition to residues in the D-helix, giving rise to more widespread chemical shift differences and enhanced amide exchange.

It is interesting to note that the A-, B-, D-, and C-terminal 3_{10}-helices form a stable core that is highly resistant to denaturant-induced unfolding in the low pH molten globule of human α-LA and that this core is stable in the absence of structure in the C-helix and β-domain (*9*). Studies of peptide models have identified residues 1−38 linked by the Cys28-Cys111 disulfide to residues 101−120 as the minimum core for a stable human α-LA molten globule (*64*); this peptide model encompasses the A-, B-, D-, and C-terminal 3_{10}-helices of α-LA. The conformational transition in native α-LA, responsible for the observed exchange broadening described in this study, may involve interconversion of the A-, B-, D-, and C-terminal 3_{10}-helices between the well-ordered native structures observed in the HT and LT crystal structures and a partially folded molten-globule-like structure. In future, ^{15}N and $^{1}H^{N}$ relaxation dispersion studies of native α-LA may provide chemical shift information that allows the nature of the interconverting structures to be described in more detail (*65*).

Harata and co-workers have suggested that the HT form, crystallized at pH 6.5 and 37 °C, with an α-helical conformation for Trp104−Cys111 represents the physiological state of α-LA (*63*). However, HSQC spectra collected for α-LA at pH 7 and 40 °C show broadening of α-domain peaks similar to that observed at pH 6.3 and 18.2 °C. This suggests that structural fluctuations within the A-, B-, D-, and C-terminal 3_{10}-helices of the α-domain are likely to be present in the physiological state of α-LA.

The α-domain of α-LA is generally defined to include residues 1−39 and 82−123, which encompass the A-, B-, C-, D-, and C-terminal 3_{10}-helices (*1*). An alternative definition of the domain structure of α-LA places the C-helix in the β-domain of the protein (α-domain residues 1−37 and 105−123, β-domain 38−104) (*66*,*67*). The ^{15}N relaxation data reported here for human α-LA, which show different behavior for the C-helix from the remainder of the α-domain, and previous hydrogen/deuterium exchange data, which show higher levels of protection for the C-helix, would appear to correlate better with the latter definition of the domain structure in the native state of α-LA.

In native α-LA, Asp87 and Asp88, near the N-terminus of the C-helix, are involved in calcium binding along with Lys79, Asp82, and Asp84 (*1*). Calcium binding to human α-LA requires the Cys61-Cys77 and Cys73-Cys91 disulfide bonds but does not require the α-domain disulfides, Cys6-Cys120 and Cys28-Cys111 (*68*). Human α-LA(β), a two-disulfide variant lacking the α-domain disulfides, has native-like levels of secondary structure in the presence of calcium. This species has tighter side-chain packing in the presence of calcium than in the molten globule formed in the absence of calcium but has substantially less well-ordered tertiary structure than the fully native state (*68*). This suggests that calcium binding to α-LA(β) results in a structured β-domain, calcium-binding loop, and C-helix while the remainder of the α-domain may be substantially more disordered (*67*,*68*). The presence of the two α-domain disulfides in native α-LA leads to stabilization of well-ordered tertiary structure throughout the α-domain. Nevertheless, the ^{15}N relaxation data presented here, and previous hydrogen/deuterium exchange data,

suggest that the A-, B-, D-, and C-terminal 3_{10}-helices of the α-domain may retain a propensity for transient unfolding to a molten-globule-like species even in the presence of the α-domain disulfide bonds.

ACKNOWLEDGMENT

We thank Peter S. Kim and Brenda A. Schulman for providing ^{15}N-labeled recombinant human α-LA for this study.

SUPPORTING INFORMATION AVAILABLE

A figure showing the assigned 750 MHz HSQC spectrum of human α-LA at pH 6.3 and 18.2 °C, a table summarizing the ^{15}N T_1, T_2, and $\{^1H\}-^{15}N$ NOE data collected at 500, 600, and 750 MHz, a table summarizing results of the Lipari−Szabo model-free analysis (model used, S^2, R_{ex}, τ_e), and a table summarizing backbone $^1H^N$ and ^{15}N chemical shifts for native human α-LA at pH 6.3. This material is available free of charge via the Internet at http://pubs.acs.org.

REFERENCES

1. Acharya, K. R., Ren, J. S., Stuart, D. I., Phillips, D. C., and Fenna, R. E. (1991) Crystal structure of human α-lactalbumin at 1.7 Å resolution. *J. Mol. Biol. 221*, 571–581.
2. Permyakov, E. A. (2005) *Alpha-Lactalbumin*, Nova Science Publishers, New York.
3. Imoto, T., Johnson, L. N., North, A. C. T., Phillips, D. C., and Rupley, J. A. (1972) Vertebrate Lysozymes, in *The Enzymes* (Boyer, P. D., Ed.) Vol. *VII*, pp 666−868, Academic Press, New York.
4. Kuwajima, K. (1989) The molten globule state as a clue for understanding the folding and cooperativity of globular-protein structure. *Proteins: Struct., Funct., Genet. 6*, 87–103.
5. Yutani, K., Ogasahara, K., and Kuwajima, K. (1992) Absence of the thermal transition in apo- α-lactalbumin in the molten globule state. A study by differential scanning microcalorimetry. *J. Mol. Biol. 228*, 347–350.
6. Peng, Z. Y., and Kim, P. S. (1994) A protein dissection study of a molten globule. *Biochemistry 33*, 2136–2141.
7. Wu, L. C., Peng, Z. Y., and Kim, P. S. (1995) Bipartite structure of the α-lactalbumin molten globule. *Nat. Struct. Biol. 2*, 281–286.
8. Schulman, B. A., Redfield, C., Peng, Z.-y., Dobson, C. M., and Kim, P. S. (1995) Different subdomains are most protected from hydrogen exchange in the molten globule and native states of human α-lactalbumin. *J. Mol. Biol. 253*, 651–657.
9. Schulman, B. A., Kim, P. S., Dobson, C. M., and Redfield, C. (1997) A residue-specific NMR view of the non-cooperative unfolding of a molten globule. *Nat. Struct. Biol. 4*, 630–634.
10. Kuwajima, K., Hiraoka, Y., Ikeguchi, M., and Sugai, S. (1985) Comparison of the transient folding intermediates in lysozyme and α-lactalbumin. *Biochemistry 24*, 874–881.
11. Ikeguchi, M., Kuwajima, K., Mitani, M., and Sugai, S. (1986) Evidence for identity between the equilibrium unfolding intermediate and a transient folding intermediate: a comparative study of the folding reactions of α-lactalbumin and lysozyme. *Biochemistry 25*, 6965–6972.
12. Arai, M., and Kuwajima, K. (1996) Rapid formation of a molten globule intermediate in refolding of α-lactalbumin. *Folding Des. 1*, 275–287.
13. Forge, V., Wijesinha, R. T., Balbach, J., Brew, K., Robinson, C. V., Redfield, C., and Dobson, C. M. (1999) Rapid collapse and slow structural reorganisation during the refolding of bovine α-lactalbumin. *J. Mol. Biol. 288*, 673–688.
14. Arai, M., Ito, K., Inobe, T., Nakao, M., Maki, K., Kamagata, K., Kihara, H., Amemiya, Y., and Kuwajima, K. (2002) Fast compaction of α-lactalbumin during folding studied by stopped-flow X-ray scattering. *J. Mol. Biol. 321*, 121–132.
15. Baum, J., Dobson, C. M., Evans, P. A., and Hanley, C. (1989) Characterization of a partly folded protein by NMR methods—Studies on the molten globule state of guinea-pig α-lactalbumin. *Biochemistry 28*, 7–13.
16. Ramboarina, S., and Redfield, C. (2003) Structural characterisation of the human α-lactalbumin molten globule at high temperature. *J. Mol. Biol. 330*, 1177–1188.
17. Wijesinha-Bettoni, R., Gao, C., Jenkins, J. A., Mackie, A. R., Wilde, P. J., Mills, E. N. C., and Smith, L. J. (2007) Heat treatment of bovine α-lactalbumin results in partially folded, disulfide bond shuffled states with enhanced surface activity. *Biochemistry 46*, 9774–9784.
18. Chyan, C. L., Wormald, C., Dobson, C. M., Evans, P. A., and Baum, J. (1993) Structure and stability of the molten globule state of guinea-pig α-lactalbumin: a hydrogen exchange study. *Biochemistry 32*, 5681–5691.
19. Kim, S., Bracken, C., and Baum, J. (1999) Characterization of millisecond time-scale dynamics in the molten globule state of α-lactalbumin by NMR. *J. Mol. Biol. 294*, 551–560.
20. Alexandrescu, A. T., Evans, P. A., Pitkeathly, M., Baum, J., and Dobson, C. M. (1993) Structure and dynamics of the acid-denatured molten globule state of α-lactalbumin: a two-dimensional NMR study. *Biochemistry 32*, 1707–1718.
21. Ramboarina, S., and Redfield, C. (2008) Probing the effect of temperature on the backbone dynamics of the human α-lactalbumin molten globule. *J. Am. Chem. Soc. 130*, 15318–15326.
22. Ewbank, J. J., and Creighton, T. E. (1993) Structural characterization of the disulfide folding intermediates of bovine α-lactalbumin. *Biochemistry 32*, 3694–3707.
23. Schulman, B. A., and Kim, P. S. (1996) Proline scanning mutagenesis of a molten globule reveals non-cooperative formation of a protein's overall topology. *Nat. Struct. Biol. 3*, 682–687.
24. Wu, L. C., and Kim, P. S. (1998) A specific hydrophobic core in the α-lactalbumin molten globule. *J. Mol. Biol. 280*, 175–182.
25. Smith, L. J., Dobson, C. M., and van Gunsteren, W. F. (1999) Molecular dynamics simulations of human α-lactalbumin: changes to the structural and dynamical properties of the protein at low pH. *Proteins 36*, 77–86.
26. Troullier, A., Reinstadler, D., Dupont, Y., Naumann, D., and Forge, V. (2000) Transient non-native secondary structures during the refolding of α-lactalbumin detected by infrared spectroscopy. *Nat. Struct. Biol. 7*, 78–86.
27. Vendruscolo, M., Paci, E., Karplus, M., and Dobson, C. M. (2003) Structures and relative free energies of partially folded states of proteins. *Proc. Natl. Acad. Sci. U.S.A. 100*, 14817–14821.
28. Koga, K., and Berliner, L. J. (1985) Structural elucidation of a hydrophobic box in bovine α-lactalbumin by NMR: nuclear Overhauser effects. *Biochemistry 24*, 7257–7262.
29. Wijesinha-Bettoni, R., Dobson, C. M., and Redfield, C. (2001) Comparison of the structural and dynamical properties of holo and apo bovine α-lactalbumin by NMR spectroscopy. *J. Mol. Biol. 307*, 885–898.
30. Kim, S., and Baum, J. (1998) Electrostatic interactions in the acid denaturation of α-lactalbumin determined by NMR. *Protein Sci. 7*, 1930–1938.
31. Alexandrescu, A. T., Broadhurst, R. W., Wormald, C., Chyan, C. L., Baum, J., and Dobson, C. M. (1992) 1H-NMR assignments and local environments of aromatic residues in bovine, human and guinea pig variants of α-lactalbumin. *Eur. J. Biochem. 210*, 699–709.
32. Buck, M., Boyd, J., Redfield, C., MacKenzie, D. A., Jeenes, D. J., Archer, D. B., and Dobson, C. M. (1995) Structural determinants of protein dynamics: analysis of ^{15}N NMR relaxation measurements for main-chain and side-chain nuclei of hen egg white lysozyme. *Biochemistry 34*, 4041–4055.
33. Chamberlain, A. K., Receveur, V., Spencer, A., Redfield, C., and Dobson, C. M. (2001) Characterization of the structure and dynamics of amyloidogenic variants of human lysozyme by NMR spectroscopy. *Protein Sci. 10*, 2525–2530.
34. Redfield, C., Schulman, B. A., Milhollen, M. A., Kim, P. S., and Dobson, C. M. (1999) α-Lactalbumin forms a compact molten globule in the absence of disulfide bonds. *Nat. Struct. Biol. 6*, 948–952.
35. Wilkins, D. K., Grimshaw, S. B., Receveur, V., Dobson, C. M., Jones, J. A., and Smith, L. J. (1999) Hydrodynamic radii of native and denatured proteins measured by pulse field gradient NMR techniques. *Biochemistry 38*, 16424–16431.
36. Kataoka, M., Kuwajima, K., Tokunaga, F., and Goto, Y. (1997) Structural characterization of the molten globule of α-lactalbumin by solution X-ray scattering. *Protein Sci. 6*, 422–430.
37. Marion, D., Driscoll, P. C., Kay, L. E., Wingfield, P. T., Bax, A., Gronenborn, A. M., and Clore, G. M. (1989) Overcoming the overlap problem in the assignment of ^{1}H NMR spectra of larger proteins by use of three-dimensional heteronuclear ^{1}H-^{15}N

Hartmann-Hahn-multiple quantum coherence and nuclear Overhauser-multiple quantum coherence spectroscopy: application to interleukin 1 beta. *Biochemistry 28*, 6150–6156.
38. Driscoll, P. C., Clore, G. M., Marion, D., Wingfield, P. T., and Gronenborn, A. M. (1990) Complete resonance assignment for the polypeptide backbone of interleukin 1 beta using three-dimensional heteronuclear NMR spectroscopy. *Biochemistry 29*, 3542–3556.
39. Ikura, M., Bax, A., Clore, G. M., and Gronenborn, A. M. (1990) Detection of nuclear Overhauser effects between degenerate amide proton resonances by heteronuclear three-dimensional NMR spectroscopy. *J. Am. Chem. Soc. 112*, 9020–9022.
40. Kay, L. E., Torchia, D. A., and Bax, A. (1989) Backbone dynamics of proteins as studied by nitrogen-15 inverse detected heteronuclear NMR spectroscopy: application to staphylococcal nuclease. *Biochemistry 28*, 8972–8979.
41. Boyd, J., Hommel, U., and Campbell, I. D. (1990) Influence of cross-correlation between dipolar and anisotropic chemical shift relaxation mechanisms upon longitudinal relaxation rates of nitrogen-15 in macromolecules. *Chem. Phys. Lett. 175*, 477–482.
42. Palmer, A. G.III, Skelton, N. J., Chazin, W. J., Wright, P. E., and Rance, M. (1992) Suppression of the effects of cross correlation between dipolar and anisotropic chemical-shift relaxation mechanisms in the measurement of spin-spin relaxation rates. *Mol. Phys. 75*, 699–711.
43. Tjandra, N., Feller, S. E., Pastor, R. W., and Bax, A. (1995) Rotational diffusion anisotropy of human ubiquitin from ^{15}N NMR relaxation. *J. Am. Chem. Soc. 117*, 12562–12566.
44. Lipari, G., and Szabo, A. (1982) Model-free approach to the interpretation of nuclear magnetic resonance relaxation in macromolecules. 1. Theory and range of validity. *J. Am. Chem. Soc. 104*, 4546–4559.
45. Lipari, G., and Szabo, A. (1982) Model-free approach to the interpretation of nuclear magnetic resonance relaxation in macromolecules. 2. Analysis of experimental results. *J. Am. Chem. Soc. 104*, 4559–4570.
46. Abragam, A. (1961) *The Principles of Nuclear Magnetism*, Clarendon Press, Oxford.
47. Ren, J., Stuart, D. I., and Acharya, K. R. (1993) α-Lactalbumin possesses a distinct zinc binding site. *J. Biol. Chem. 268*, 19292–19298.
48. Cornilescu, G., and Bax, A. (2000) Measurement of proton, nitrogen, and carbonyl chemical shielding anisotropies in a protein dissolved in a dilute liquid crystalline phase. *J. Am. Chem. Soc. 122*, 10143–10154.
49. Boyd, J., and Redfield, C. (1998) Defining the orientation of the N-15 shielding tensor using N-15 NMR relaxation data for a protein in solution. *J. Am. Chem. Soc. 120*, 9692–9693.
50. Boyd, J., and Redfield, C. (1999) Characterization of N-15 chemical shift anisotropy from orientation-dependent changes to N-15 chemical shifts in dilute bicelle solutions. *J. Am. Chem. Soc. 121*, 7441–7442.
51. Findeisen, M., Brand, T., and Berger, S. (2007) A ^{1}H-NMR thermometer suitable for cryoprobes. *Magn. Reson. Chem. 45*, 175–178.
52. Mandel, A. M., Akke, M., and Palmer, A. G.III (1995) Backbone dynamics of *Escherichia coli* ribonuclease HI: correlations with structure and function in an active enzyme. *J. Mol. Biol. 246*, 144–163.
53. Clore, G. M., Szabo, A., Bax, A., Kay, L. E., Driscoll, P. C., and Gronenborn, A. M. (1990) Deviations from the simple two-parameter model-free approach to the interpretation of nitrogen-15 nuclear magnetic relaxation of proteins. *J. Am. Chem. Soc. 112*, 4989–4991.
54. Millet, O., Loria, J. P., Kroenke, C. D., Pons, M., and Palmer, A. G. III (2000) The static magnetic field dependence of chemical exchange linebroadening defines the NMR chemical shift time scale. *J. Am. Chem. Soc. 122*, 2867–2877.
55. Johnson, M. L., and Faunt, L. M. (1992) Parameter estimation by least-squares methods. *Methods Enzymol. 210*, 1–37.
56. Redfield, C., and Dobson, C. M. (1988) Sequential proton NMR assignments and secondary structure of hen egg white lysozyme in solution. *Biochemistry 27*, 122–136.
57. Redfield, C., and Dobson, C. M. (1990) Proton NMR studies of human lysozyme: spectral assignment and comparison with hen lysozyme. *Biochemistry 29*, 7201–7214.
58. Harata, K., Abe, Y., and Muraki, M. (1999) Crystallographic evaluation of internal motion of human α-lactalbumin refined by full-matrix least-squares method. *J. Mol. Biol. 287*, 347–358.
59. Phan, I. Q. H., Boyd, J., and Campbell, I. D. (1996) Dynamic studies of a fibronectin type I module pair at three frequencies: anisotropic modeling and direct determination of conformational exchange. *J. Biomol. NMR 8*, 369–378.
60. Buck, M., Bouguet-Bonnet, S., Pastor, R. W., and MacKerell, A. D. Jr. (2006) Importance of the CMAP correction to the CHARMM22 protein force field: dynamics of hen lysozyme. *Biophys. J. 90*, L36–L38.
61. Radford, S. E., Buck, M., Topping, K. D., Dobson, C. M., and Evans, P. A. (1992) Hydrogen exchange in native and denatured states of hen egg-white lysozyme. *Proteins 14*, 237–248.
62. Canet, D., Last, A. M., Tito, P., Sunde, M., Spencer, A., Archer, D. B., Redfield, C., Robinson, C. V., and Dobson, C. M. (2002) Local cooperativity in the unfolding of an amyloidogenic variant of human lysozyme. *Nat. Struct. Biol. 9*, 308–315.
63. Harata, K., and Muraki, M. (1992) X-ray structural evidence for a local helix-loop transition in α-lactalbumin. *J. Biol. Chem. 267*, 1419–1421.
64. Demarest, S. J., Boice, J. A., Fairman, R., and Raleigh, D. P. (1999) Defining the core structure of the α-lactalbumin molten globule state. *J. Mol. Biol. 294*, 213–221.
65. Vallurupalli, P., Hansen, D. F., and Kay, L. E. (2008) Structures of invisible, excited protein states by relaxation dispersion NMR spectroscopy. *Proc. Natl. Acad. Sci. U.S.A. 105*, 11766–11771.
66. Siddiqui, A. S., and Barton, G. J. (1995) Continuous and discontinuous domains: an algorithm for the automatic generation of reliable protein domain definitions. *Protein Sci. 4*, 872–884.
67. Hendrix, T. M., Griko, Y., and Privalov, P. (1996) Energetics of structural domains in α-lactalbumin. *Protein Sci. 5*, 923–931.
68. Wu, L. C., Schulman, B. A., Peng, Z. Y., and Kim, P. S. (1996) Disulfide determinants of calcium-induced packing in α-Lactalbumin. *Biochemistry 35*, 859–863.
69. Pettersen, E. F., Goddard, T. D., Huang, C. C., Couch, G. S., Greenblatt, D. M., Meng, E. C., and Ferrin, T. E. (2004) UCSF Chimera—A visualization system for exploratory research and analysis. *J. Comput. Chem. 25*, 1605–1612.